J Bionic Eng 15 (2018) 220–235
DOI: https://doi.org/10.1007/s42235-018-0017-9

Journal of Bionic Engineering
http://www.springer.com/journal/42235

A Soft Bionic Gripper with Variable Effective Length

Yufei Hao[1], Zheyuan Gong[1], Zhexin Xie[1], Shaoya Guan[1], Xingbang Yang[1,2], Tianmiao Wang[1], Li Wen[1,3*]

1. *School of Mechanical Engineering and Automation*, *Beihang University*, *Beijing* 100191, *China*
2. *School of Biological Science and Medical Engineering*, *Beihang University*, *Beijing* 100191, *China*
3. *Beijing Advanced Innovation Center for Biomedical Engineering*, *Beihang University*, *Beijing* 100191, *China*

Abstract

This article presented a four-fingered soft bionic robotic gripper with variable effective actuator lengths. By combining approaches of finite element analysis, quasi-static analytical modeling, and experimental measurements, the deformation of the single soft actuator as a function of air pressure input in free space was analyzed. To investigate the effect of the effective actuator length on the gripping performance of the gripper, we conducted systematical experiments to evaluate the pull-off force, the actuation speed, the precision and error tolerance of the soft gripper while grasping objects of various sizes and shapes. A combination of depressurization and pressurization in actuation as well as applying variable effective actuator length enhanced the gripper's performance significantly, with no sensors. For example, with tunable effective actuator length, the gripper was able to grasp objects ranging from 2 mm – 170 mm robustly. Under the optimal length, the gripper could generate the maximum pull-off force for the corresponding object size; the precision and the error tolerance of the gripper were also significantly improved compared to those of the gripper with full-length. Our soft robotic prototype exhibits a simple control and low-cost approach of gripping a wide range of objects and may have wide leverage for future industrial operations.

Keywords: soft robotics, pneumatic control, soft bionic gripper, variable effective actuator length

1 Introduction

Soft robotics is a new member of the robotic family that has several promising features, such as lightweight, low cost, easy fabrication, simple control[1–3]. Recently, researchers from multiple disciplines have devoted to the research on the material[4,5], modeling[6,7], and robotic prototypes[8,9] of soft robotics. Several new methods, including multi-material 3D printing[10,11], soft lithography[12–14] and integrated multiple manufacturing methods to create composite materials[15–17], were introduced to fabricate complicated soft robots. Besides the traditional variable-length tension cables driving[18,19], new actuation methods, such as pneumatic or hydraulic actuation[12,20], dielectric elastomer[21], and electroactive polymer[22], have been introduced to actuate soft robots. Although there exist many unsolved problems in soft robotics, several potential applications have been achieved, for example, the wearable personal rehabilitation device[23,24], bio-inspired robotic locomotion[12,25,26], and human-machine interaction[2].

The conventional rigid robotic gripper typically uses two or more fingers that require visual feedback and force sensing at the fingertips and a central processor running algorithms to make decisions before gripper touches the object for achieving adaptive gripping[18]. Therefore, the rigid multi-fingered gripper is a complex system to implement and control. While a universal gripper based on soft material actuation may have a variety of application scenarios where objects with different sizes and shapes need to be gripped reliably and in rapid succession[8,18]. Recently, soft pneumatic grippers have attracted many researchers' attention for the inherent safety[27–29]. However, these grippers can only bend in one direction. To further open the grasping space, the depressurization and pressurization mechanism have been applied to the soft actuator to generate bi-directional bending motion, which may significantly improve the grasping performance[30–32]. However, recent works mainly focus on the geometrical parameter optimization, the dexterous demonstration or the fabrication methods[33] of the soft gripper. Few quantitative

***Corresponding author:** Li Wen
E-mail: liwen@buaa.edu.cn

studies for the industrial application have been provided, and many questions remain: what is the maximum gripping force that a soft pneumatic gripper can output? Can the sizes and shapes of the objects influence the gripping performance of the gripper and what is the relationship of these parameters? Are there any fundamental mechanisms for explaining the gripping performance? To scientifically address the questions above, we should conduct systematic experiments to test the gripping performance of the soft gripper quantitatively. To our knowledge, little systematic characterization has been carried out for a soft robotic prototype on gripping objects with different sizes, shapes or material stiffness.

In this article, we designed a soft gripper that contains four pneumatic elastomeric actuators incorporating both positive and negative pressures, which may increase its actuation speed. This gripper only requires simple control for pneumatic actuation: deflating the soft actuators to open the gripper "jaw" and approach the objects, then inflating the actuators to conform the gripped objects. We used a selectively-placed inelastic nylon tendon to change the deformation area of actuator mechanically (we term the length of this area as "effective actuator length" of the soft gripper), and quantified the effective actuator lengths and pull-off forces while the gripper grasped objects with different shapes and sizes under certain air pressures. By attaching the prototype to a commercial robot arm, we also investigated the effect of effective actuator length on the actuation speed, the precision of the gripper for picking and placing, as well as the gripper's ability to tolerate errors when grasping objects. Based on the experimental results, we formulated several hypotheses of the gripping mechanisms and concluded that this gripper might have a variety of potential applications. This paper primarily focuses on (1) design and fabricate a soft robotic actuator through FEA and theoretical analysis; (2) quantitatively test the pull-off forces, the actuation speed, the precision and error tolerance of a four-fingered soft gripper under different effective actuator lengths while grasping objects with different sizes and shapes.

2 Materials and methods

2.1 Design, fabrication and FEA of the soft actuator

The single actuator consists of an extensible top layer and inextensible, but flexible bottom layer (see Step 5 of Fig. 1). When actuated, the expansion or contraction of the two neighboring chambers causes a preferential elongation or reduction of the extensible top layer, with minuscule change in the height of this layer. Meantime, the bottom layer has to bend to adapt this deformation because it is inextensible. We term the typical chamber structure as a "depressurization & pressurization actuator unit". Each chamber of the actuator has a chamber width of 20 mm, a wall height of 20 mm and a wall thickness of 1.3 mm. There are 13 chambers in the actuator with a total length of 106 mm under no deformation.

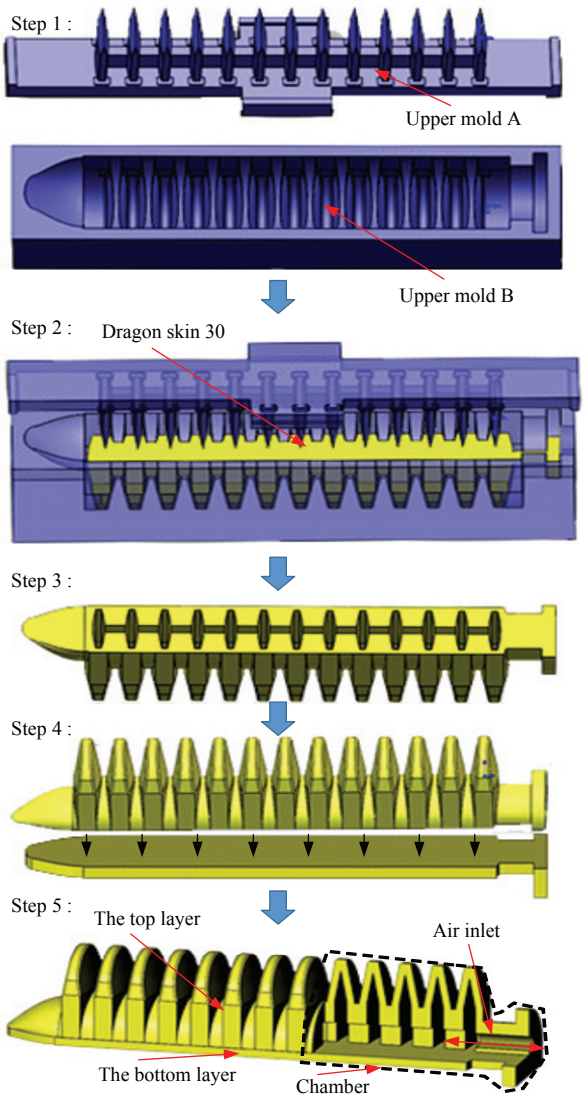

Fig. 1 Schematic of the fabrication process of a single soft actuator.

The soft actuator was fabricated using silicon rubber material (dragon skin 30, smooth-on Inc., America).

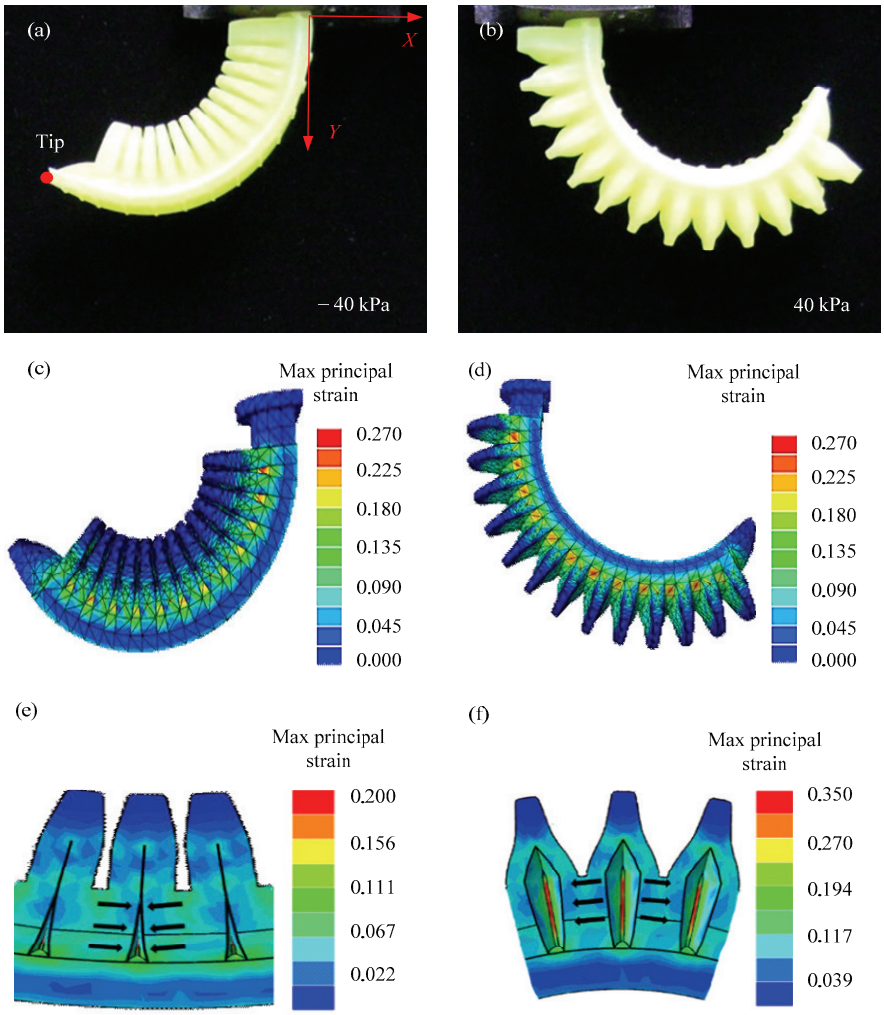

Fig. 2 Kinematics comparison between simulation and experiment for a single soft actuator. (a) and (b) show the deformation of the actuator under the pressure of −40 kPa and 40 kPa separately, while (c) and (d) show the corresponding simulation results. (e) and (f) show the enlarged detail of the depressurization and pressurization states.

The rigid molds were designed in Solidworks (Solid Works Corp., Waltham, MA, USA) and fabricated using PLA material by 3D printing. The simplified process allowed us to iterate the fabrication quickly. The multi-step molding process of a single soft actuator was shown in Fig. 1. Note that the fabrication process was inspired from the manufacture of Harvard pneumatic-net soft robotic actuators[14]. The upper molds A and B were fabricated to form the extensible and contractible top layer that contains topographical features (Step 1 of Fig. 1). Firstly, the uncured silicone rubber material was poured into the upper mold B (Step 2 of Fig. 1). The mold and uncured material were then settled in a vacuum oven for 30 minutes for degassing, thus to remove the air bubbles, and were then heated to a temperature of 60 ˚C for 2 hours to cure the silicone material. Finally, the top layer was unmolded (Step 3 of Fig. 1) and then sealed with the bottom layer by applying a thin layer of uncured silicone rubber on the bonding surface (Step 4 of Fig. 1). By inflating or deflating, the soft actuator that contains topographical feature would expand or contract, which further results in bending in either convex or concave state (see Fig. 2a and Fig. 2b for notation).

From Fig. 2, it can be observed that the simulation results agree well with the experiments. In supplementary video S1, the comparison between experiment and simulation of a single actuator under pressurization and depressurization shows good agreement[34]. For the

simulation conditions, finite element simulations were performed using the commercial finite element software Abaqus (Abaqus 6.12, SIMULIA Inc., France). The elastomer was modeled as an incompressible Mooney-Rivlin material *via* the hyperelastic Mooney-Rivlin model with an elastic modulus (E) of 1 Mpa[35] and the Poisson ratio (μ) of 0.49. For the elastomer, 10-node quadratic tetrahedron, with hybrid formulation (Abaqus element type C3D10H), was used. The accuracy of the mesh was ascertained through a mesh refinement study and a simplification of the model. Each simulation required 22,378 elements and 39,884 nodes. Quasi-static nonlinear simulations were performed using Abaqus/Standard. One end of the actuator was fixed both in the translation and rotation directions, and the pressure load was applied to the inner surface of the actuator.

2.2 Modeling of the soft actuator

A theoretical model was developed for describing the relationship between air pressure input and actuator fingertip deformation output. Note that the actuation of the soft actuator was realized by two main mechanisms: the pressurization and the depressurization of the chamber under different pressures. To derive the theoretical model of a single soft actuator, we assume that 1) the flat bottom layer (see Fig. 1 for notation) would not elongate or shorten during the deformation and 2) there exists no radial inflation for all the chambers during deformation. As we designed all the 13 chambers with the same geometry, the soft actuator was separated into 13 sections to calculate the displacements individually and then integrated to obtain the tip displacement. For each section, the length in the x direction was defined as k, and the displacements x_i and y_i were calculated through the combination of two bending angles (see Fig. 3e for notation). The angle β was generated by the inflating/deflating of the top layer, and the other angle γ was caused by the bending of the bottom layer. Two separate mechanical models were established to calculate the two angles.

We used the quasi-static model to evaluate the dynamics of the single soft actuator. When the air was inflated into the chambers of the soft actuator, the gap between the neighboring walls expanded from s_1 to s_2 (see Fig. 3a and Fig. 3b for notation), and the section unit bent into an angle of β. The following equation can be established to calculate β:

$$\tan\frac{\beta}{2}=\frac{w_{1\max}}{l_1}, \tag{1}$$

where $w_{1\max}=|s_1-s_2|/2$. From Fig. 3c, the walls of the chamber can be considered as curve plate with simple support edges. The deflection differential equation for a plate model was:

$$D\nabla^4 w=q, \tag{2}$$

where D indicates the flexural rigidity of the plate and can be calculated as $Eh^3/12(1-\mu^2)$. In this formula, h indicates the thickness of the plate (chamber wall). E and μ are separately the elastic modulus and Poisson ratio of the material. q indicates the force distributed on the inner side wall of the soft actuator per unit area and equals the input air pressure P. w indicates deflection of the soft actuator unit in general. In particular, deflections of the soft actuator unit exhibited along x and z directions, while the deflection in the y direction was tiny and can be ignored. More specifically, deflection in the x and z direction can be denoted as w_1 and w_2 respectively.

The cross section of the inner chamber is symmetric along the z direction (see Fig. 3a). Therefore we focused on the half side of the chamber, and its schematic view is described in Fig. 3c. The geometrical feature of the inner chamber resembled an overall shape of "rocket", therefore we divided the curve plate, which indicates one side of the inner chamber, into two segments: AB and BC shown in Fig. 3b. The AB segment has a rectangle shape with the length (in the z direction) of l_1 and the width (in the y direction) of b. To simplify the model of section BC, we considered the semicircle as a rectangle which has the same area. The simplified BC segment has a length of l_2 and shares the same width b as that of section AB. The boundary conditions of the force model of AB and BC sections were shown as:

$$w_1=0 \quad \text{at } z=0, z=l_1+l_2, y=0, y=b \tag{3}$$

$$\frac{\partial^2 w_1}{\partial z^2}+u\frac{\partial^2 w_1}{\partial y^2}=0 \quad \text{at } z=0, l_1+l_2 \tag{4}$$

$$\frac{\partial^2 w_1}{\partial y^2}+u\frac{\partial^2 w_1}{\partial z^2}=0 \quad \text{at } y=0, b. \tag{5}$$

According to Navier method[36], the deflection of the plate can be expressed as a double Fourier series:

$$w_1 = \sum_{i=1}^{\infty}\sum_{j=1}^{\infty} A_{ij} \sin\frac{i\pi z}{l_1 + l_2} \sin\frac{j\pi y}{b}, \tag{6}$$

where A_{ij} is a parameter related to geometrical and material features. The boundary conditions of the chamber and can be expressed as Eq. (7).

Combining Eqs. (2), (6) and (7), we could obtain

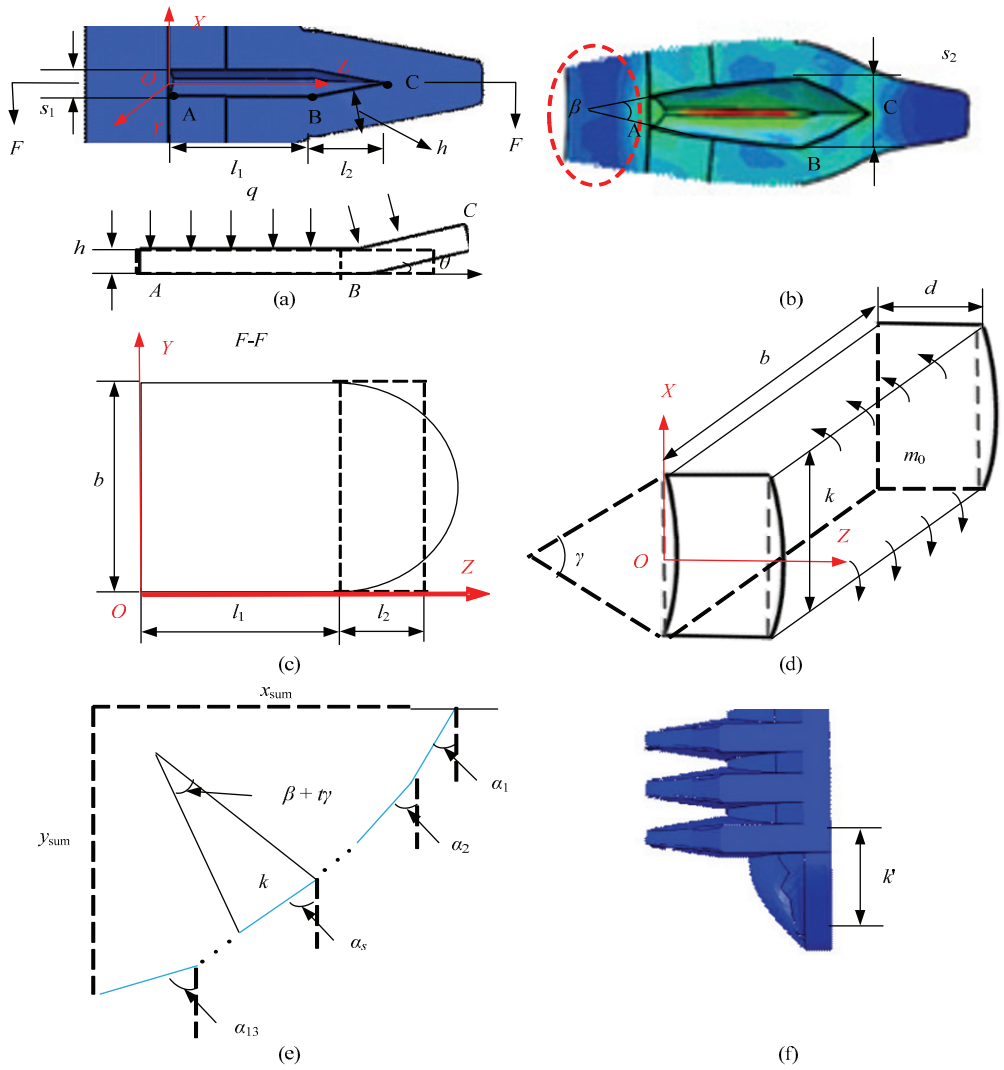

Fig. 3 The mathematical model of the soft actuator. The dimensions of one chamber before and after deformation were showed in (a) and (b). The cross-section area at the F-F line was illustrated in (c). The mathematic model for the bottom layer of one section was explained in (d). The diagrammatic integration process for the 13 sections of the model was explained in (e). The fingertip length of the actuator was explained in (f). s_1: the initial gap between the inner walls of the chamber; s_2: the gap distance under deformation; l_1: the length in the Z direction of the AB segment. l_2: the equivalent length in the Z direction of the BC segment; h: the thickness of the chamber; b: the width (in the y direction) of the chamber; k: the length of the section in the X direction; k': the fingertip length.

$$A_{ij} = \frac{\left[P\left(1-\cos\frac{l_1}{l_1+l_2}i\pi\right)+P/\cos\theta\left(\cos\frac{l_1}{l_1+l_2}i\pi-\cos i\pi\right)\right]4\left(1-\cos j\pi\right)}{\pi^6 ijD_1\left[\frac{i^2}{\left(l_1+l_2\right)^2}+\frac{j^2}{b^2}\right]^2}. \tag{7}$$

the angle β at different air pressures P. The flexural rigidity of the plate can be denoted as $D_1=Eh^3/12(1-\mu^2)$.

We also provide a schematic view of the deformed bottom layer in a three-dimensional view (as shown in Fig. 3d) for calculating angle γ which indicates the deformation of the bottom layer. The flexural rigidity of the plate can be denoted as $D_2=Ed^3/12(1-\mu^2)$, where d is the thickness of the bottom layer. The torque induced by the inner pressure was equivalent to the distributed torque m_0 at the edge of the bottom layer plate ($x=\pm k/2$). The distributed torque m_0 can be expressed as:

$$m_0=\frac{P}{2}\left(l_1+l_2\cos\theta\right)^2, \tag{7}$$

where θ is the top wedged angle of the "rocket" shaped inner chamber. The boundary conditions of the bottom layer were:

$$w_2\big|_{x=\pm\frac{k}{2}}=0, \tag{8}$$

$$-D_2\frac{\partial^2 w_2}{\partial x^2}\Big|_{x=\pm\frac{k}{2}}=m_0. \tag{9}$$

The Fourier series expansion of the m_0 can be expressed as:

$$m_0=\sum_{i=1}^{\infty}E_i\sin\frac{i\pi x}{k}. \tag{10}$$

Combining Eqs. (10) and (11), the boundary condition could be expressed as:

$$-D_2\frac{\partial^2 w_2}{\partial x^2}\Big|_{x=\pm\frac{k}{2}}=\sum_{i=1}^{\infty}E_i\sin\frac{i\pi x}{k}, \tag{11}$$

where E_i is a parameter related to a geometrical feature of the chamber and can be expressed as:

$$E_i=\frac{2m_0}{b}\int_0^b\sin\frac{i\pi y}{b}\mathrm{d}y. \tag{12}$$

The distributed torque m_0 was symmetrical about the YZ panel. According to Levy's Solution by Single Trigonometric Series[36], w_2 could be expressed as:

$$w_2=\sum_{i=1}^{\infty}\left(A_i\cosh\frac{i\pi x}{k}+B_i\frac{i\pi x}{k}\sinh\frac{i\pi x}{k}\right)\sin\frac{i\pi y}{b}, \tag{13}$$

where A_i and B_i are variables related to geometrical, material features and the boundary conditions of the chamber, and they can be expressed as:

$$A_i=-\frac{i\pi k}{2b}B_i\tanh\frac{i\pi k}{2b}, \tag{14}$$

$$B_i=-\frac{E_i}{2D_2}\frac{b^2}{i^2\pi^2}\frac{1}{\cosh\left(i\pi k/2b\right)}. \tag{15}$$

Based on the geometrical condition, the angle γ can be therefore obtained as:

$$\cos\frac{\gamma}{2}=\frac{k}{k+2w_2\big|_{x=0}}. \tag{16}$$

From Fig. 3e, the displacement of a single soft robotic unit in x and y directions can be described as:

$$\begin{aligned}&x_s=k\sin a_s=k\sin\left(a_{s-1}+\frac{\beta+t\gamma}{2}\right)=k\sin\left(\sum_{r=1}^{s}\frac{\beta+t\gamma}{2}\right),\\&y_s=k\cos\left(\sum_{r=1}^{s}\frac{\beta+t\gamma}{2}\right),\left(1\le s\le 13;1\le r\le s\right).\end{aligned} \tag{17}$$

Integrating the displacements of all the sections (there are 13 units and one tip unit in total), we could get the final tip displacement of the soft actuator:

$$\begin{aligned}x_{sum}&=\sum_{s=1}^{13}k\sin\left(\sum_{r=1}^{s}\frac{\beta+t\gamma}{2}\right)+k'\sin\left(\sum_{r=1}^{13}\frac{\beta+t\gamma}{2}\right),\\y_{sum}&=\sum_{s=1}^{13}k\cos\left(\sum_{r=1}^{s}\frac{\beta+t\gamma}{2}\right)+k'\cos\left(\sum_{r=1}^{13}\frac{\beta+t\gamma}{2}\right).\end{aligned} \tag{18}$$

where k' indicates the tip length of the soft actuator (see Fig. 3f) and t is an empirical parameter which was obtained experimentally.

Concerning the bi-directional bending feature of the soft actuator, we built a soft robotic gripper prototype for gripping objects: deflating the soft actuators to curl outwards, i.e., open the gripper "jaw" (see Fig. 4c) and approach the objects. Then the chambers will be inflated with compressed air, and the actuators will curl inwards and contact with the surface of the objects (see Fig. 4d). Further increasing the inflating air pressure would allow the gripper to conform the objects. The soft gripper was comprised of four soft actuator elements. Each of the elements primarily consists of three components (Fig. 4a): (1) the soft elastomeric actuator, (2) the fixator that is used to fasten and connect the soft actuator to the support, and was 3D printed with PLA material, (3) the tube joint that allows the compressed air to

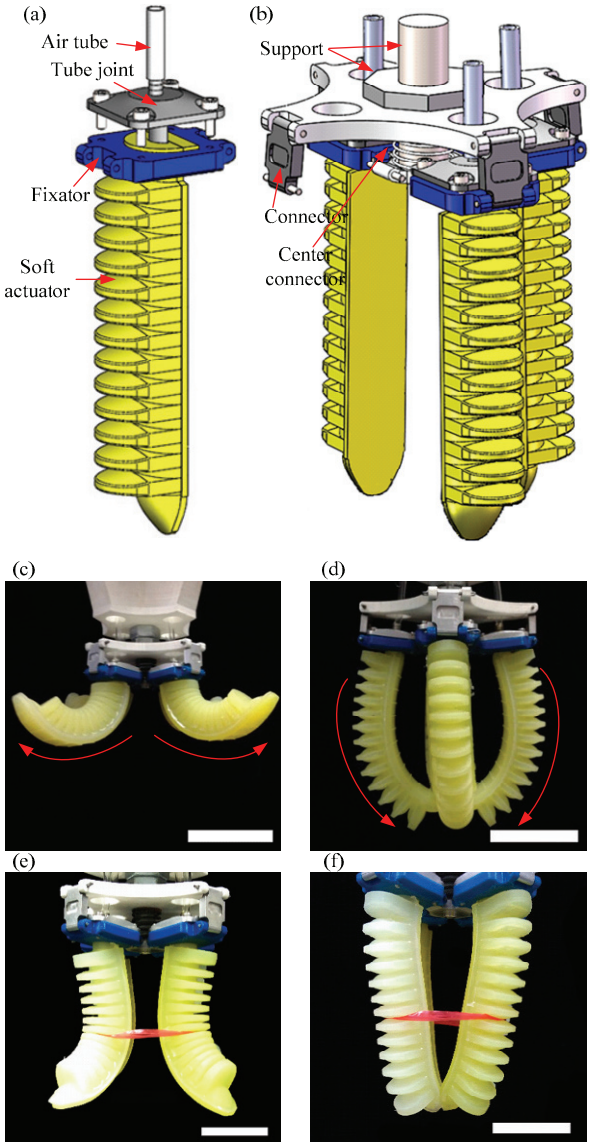

Fig. 4 The design and configuration of the soft robotic gripper. (a) and (b) show the detailed structure of the gripper. (c) and (e) show the depressurization state of the gripper under the full effective length and 50 mm effective length. (d) and (f) show the pressurization state of the gripper under the corresponding effective length. The scale bars are all 50 mm.

inflate/deflate the soft actuator. The lower part of the tube joint was inserted into the air inlet (Step 5 in Fig. 1) of the soft actuator and the other part was connected with the air tube (Fig. 4a). The tube joint and the fixator were fastened with bolts to seal the air channel and avoid air leakage. The soft actuator elements were integrated on a 3D printed rigid base support (Fig. 4b). We used a One-Touch Fitting (KQ2UD04, SMC Inc., Japan) to converge the four air tubes that connect with each of the

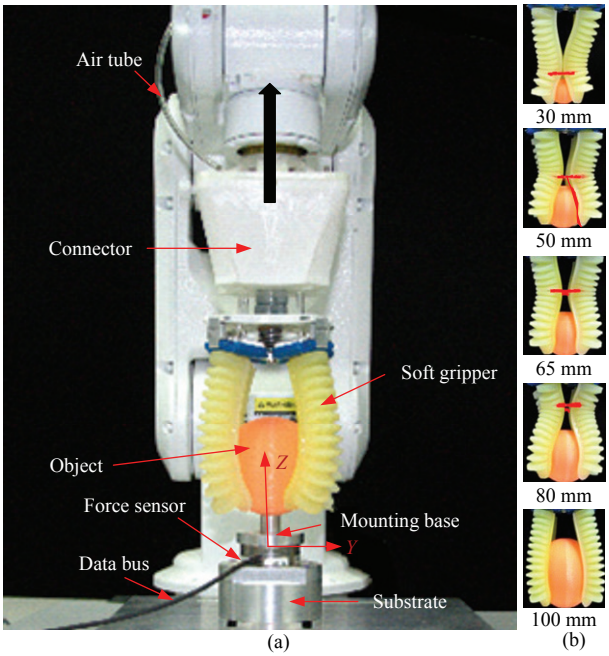

Fig. 5 Apparatus for measuring the pull-off force of the soft gripper under different effective lengths. (a) shows the schematic illustration of the force measurement platform, and (b) shows the five selected effective lengths (the red dashed line in the pictures).

four soft actuators to a single air inlet tube. Therefore, all actuators could be inflated simultaneously. The single air inlet tube was connected to an electro-pneumatic proportional pressure valve (ITV0030, SMC Inc., Japan) which was used to control the output air pressure by changing the voltage input. In addition, we used a selectively-placed inelastic nylon tendon that acts to modify the actuator area of pressurization and depressurization mechanically (see Fig. 4e and Fig. 4f for notation). We termed the length of this area as "effective actuator length of the soft gripper" (also shown in Fig. 5b).

2.3 Experimental setup for characterizing the gripping performance

To evaluate the gripping performance of the prototype, we set up an experimental platform to test the pull-off force of the gripper when grasping different objects. To this end, we kept the object fixed and pulled the gripper vertically up at a constant speed. As shown in Fig. 5a, the gripped object was connected to a six-axis force transducer (Mini 40 F/T sensor, ATI, America) via a mounting base. The bottom side of the force transducer

was mounted to an optical table through the substrate. The robotic arm (MOTOMAN MH3F, YASKAWA Inc., Japan) moved vertically upward, therefore, to pull the soft gripper up and away from the gripped object. During each experimental trial, we first biased the weight of the object in a force data acquisition system using a Labview program. Then the soft actuators would be inflated to a preset pressure and conform the test object. Afterward, the gripper was moved upward at a constant speed of 18 $mm \cdot s^{-1}$ until the gripper was completely detached from the object, which took about 5 s. During the gripping process, the force data along Z axis was recorded simultaneously at a sampling rate of 500 Hz. Then the force data was filtered by a low-pass filter (15 Hz). The average value of 5 maximum peak forces was finally used for calculating the pull-off force of each measurement. Here in this study, the pull-off force was defined as the maximum force generated during the whole gripping process.

To test the relationship between pull-off force and the size of the gripped objects as well as the variable effective actuator lengths, we 3D printed eight rigid spheres with different diameters, ranging from 20 mm to 90 mm with an interval of 10 mm. While characterizing the force performance, different effective actuator lengths (30 mm, 50 mm, 65 mm, 80 mm, and 100 mm) were selected before the test for each gripped object (see Fig. 5b for notation). In addition, three air pressures were chosen to inflate the soft gripper (30 kPa, 50 kPa, and 70 kPa). For each test, we pre-set the pressure and the effective actuator length of the soft gripper according to the parameters we selected, then used the gripper to grasp the eight objects in the order of increasing diameter of the spheres. For this experiment, over 120 experimental cases were conducted, and five repeated trials were performed for each case to obtain the mean data. To sum up, over 600 trials were carried out. We also performed pull-off force experiments to investigate the effect of the shapes of gripped objects. Six objects with different shapes but equal circumscribed spheres (sphere, cylinder, cuboid, cube, eight-angular prism and square pyramid) were 3D printed using PLA material. Then we tested the pull-off force for each of the objects above under a fixed effective actuator length (100 mm) and air pressure (50 kPa).

The actuation speed, error tolerance and the precision of the soft gripper are essential parameters for industrial applications. A higher actuation speed can contribute to a higher efficiency of operation. A larger error tolerance when gripping the objects and greater precision when placing the objects would significantly reduce the complex requirements for the control system and algorithm. Therefore, we conducted three systematic experiments to characterize these parameters.

For the actuation speed experiment, the end of the robot arm kept a height of 0.45 m above the objects, ensuring that the tip of the gripper could touch the ground. Here the actuation speed was measured by the actuation time, which was defined as the period from pressurizing the deflated soft gripper to getting into a state that the gripper completely conforms the object and stops moving. A video recorded the whole gripping process and the actuation time was extracted via the post video process. For this process, we compared the successive frames of the video to get the frame that the gripper stopped deformation. The actuation time was then calculated by the frame number multiplied by the reciprocal of the frame frequency. Two tests were conducted for this experiment. The first one was to test the effects of the shape of the objects and the applied pressure on the actuation speed. Thus, four objects with different shapes, i.e., the sphere with the diameter of 60 mm, the eight-angular prism, the square pyramid, and the cube, were chosen as the target objects, and the actuation pressures were 30 kPa and 40 kPa respectively. The second test was to test the effect of the effective actuator length and the object size on actuation speed. For this aim, three spheres with diameters of 40 mm, 50 mm and 60 mm were selected. We chose the effective lengths as 100 mm (the full actuator length) and the optimal length for the specific sphere. The optimal length was defined as the effective length under which the gripper can generate the maximum force when gripping an object with a particular size. Based on the results of the pull-force test, the optimal lengths are 50 mm, 65 mm and 80 mm for the diameters of 40 mm, 50 mm and 60 mm in sequence. The air pressure in this test was set as 30 kPa.

For the precision experiment, the robot arm was programmed to execute a picking-placing route for two

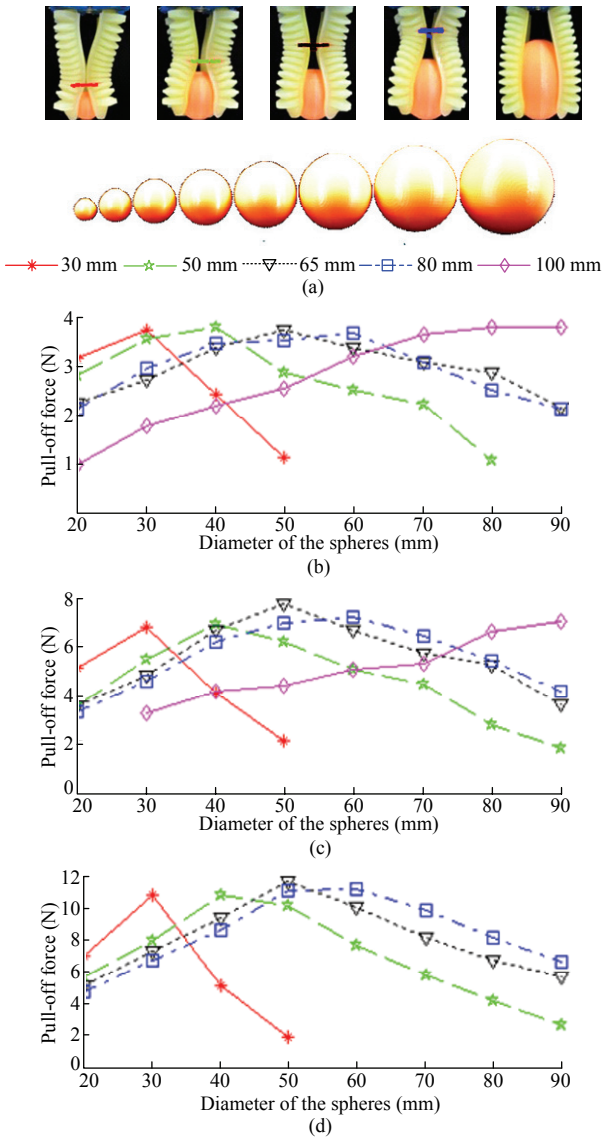

Fig. 6 Pull-off force versus the diameter of the sphere as a function of effective actuator lengths under pneumatically actuated pressures of (b) 30 kPa, (c) 50 kPa and (d) 70 kPa. The legend is shown in (a).

spheres (30 mm and 60 mm diameters respectively). The full length and the optimal length were selected for each sphere to evaluate their effects on the precision. Totally 40 trials were conducted for this experiment. For each trial, the gripper arrived at location A to pick up the object, then moved to location B to place the object. After placing, the position of the object was captured by a camera (aca1600-60gc, BASLER Inc., Germany) right above the object and the coordinate of the geometrical center of the object was identified by a vision program in Labview (NI Vision Builder, National Instrument Inc., USA).

The aim of the error tolerance experiment was to evaluate the tolerance to errors in the picking location of the target object. Two parameters were tested: the offset "Δo" and the height "Δh". "Δo" represented the distance between the center axis of the soft gripper and the sphere while "Δh" indicated the height from the fingertips of the gripper to the ground. In this experiment, the gripper was set to pick up a 70 mm diameter sphere with the mass about 200 g, which is a typical weight for many light industrial applications. For each value of the two parameters, 20 trials were conducted. During each trial, the gripper was firstly actuated to pick up the object, then the robot arm moved perpendicularly upward 40 mm at a speed of 30 mm·s^{-1} and suspended for 4 seconds after that. If the object did not drop down during the entire process, this process was predicated as a successful trial. Then the successful rates were acquired according to the statistical results. The offset error tolerance Δo was evaluated under different pressures. The pressures in this test were 40 kPa and 50 kPa respectively, and the effective actuator length was 100 mm. The height error tolerance Δh was appraised under different effective actuator lengths while the Δo was kept zero. The selected effective lengths were 100 mm and 65 mm respectively, and the pressure in the test was kept 40 kPa. Finally, to validate the universality of the soft gripper, we used it to grip some common commodities or items with different sizes, shapes, and stiffness.

3 Results and discussion

3.1 Effects of the effective actuator length on the gripping performance

Fig. 6 shows the pull-off force results as a function of the sizes of the objects, the effective actuator lengths, and the air pressures. It can be observed that, except the case of 100 mm length, the pull-off forces under the other four lengths exhibit a profile shape of "parabola" which gradually increases to a maximum peak and then decreases as the sphere diameter increases. Therefore, there exists an optimal length with the maximum pull-off force for a specific size. It is quite noteworthy that the peak values of the five curves appear at different diameters. Specifically, soft gripper with longer/shorter effective length prefers larger/smaller diameter of the spheres. It may be due to the constant deformation

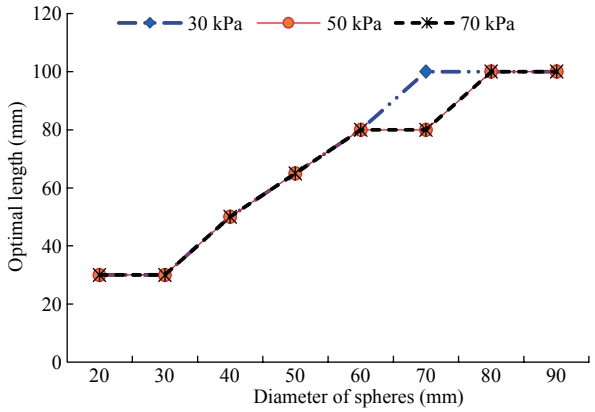

Fig. 7 The optimal length as a function of the diameter of spheres under different pressures.

curvature of the soft actuator. For a certain object, if the length of the actuator is not sufficient, the gripper cannot fully conform the object. However, if the actuator is too long, the deformation curvature of the actuator will be much bigger than the diameter of the sphere, causing that the gripper cannot entirely contact the surface of the gripper either. So we speculate that for a specific diameter sphere, it would be better that the curvature of the deformed actuator is similar to that of the sphere. It is also quite interesting that, under the same air pressure, the maximum forces were approximate for different effective lengths, which means the diameters of sphere do not significantly affect the peak values of pull-off force. We speculated that the maximum force was constrained by the material and the structure of the soft gripper. From Fig. 6b to Fig. 6d, when air pressure increases from 30 kPa to 70 kPa, the average pull-off forces increase by around three times. However, the optimal lengths kept the same under different pressures except for the 70 mm sphere, which demonstrates that the optimal length is not related to the pressure.

Based on the results of pull-off force, we concluded a function for the relationship between the optimal actuator length and the objects' size. As shown in Fig. 7, the optimal length demonstrates a rising tendency with the growth of the diameter, except for some points. It may be due to the optimal length selected is not the excellent match for the diameter. However, once we know the size, we can still use this function to choose an optimal length for the object. For the automatic control applications, in the future, we can establish a gripping control algorithm (such as the fuzzy control algorithm) based on the data of pull-off force experiments. One can imagine that we can easily grip objects with different sizes by setting the soft robotic gripper to the optimal length for the object size, instead of changing the whole manipulator. Therefore, we consider that the soft robotic gripper with tunable effective actuator lengths may have potential applications in many industrial manipulations.

To verify the simulation and mathematical model results, we inflated the soft actuator to a certain pressure and characterized the kinematics of the actuator under different pressures ranging from −40 kPa to 40 kPa. Then we digitized the tip displacements of the soft actuator in the coordinate system shown in Fig. 2a and compared them with the simulation and mathematical results. Two effective actuator lengths were conducted: one was 106 mm (the full length), and the other was 50 mm. From Fig. 8, we found that the simulation and math model results agree well with the experimental results at lower pressure values. However, the results deviate that of the experiment gradually when the absolute pressure value turns bigger. This situation may be caused by the nonlinearity of the material and the irregular geometric shape. The errors between the mathematical model and the results of the experiment turn much bigger when the pressure deviates further from the zero point. The deformation of the actuator is huge under bigger pressures, which cannot be perfectly described by the math model. The large deformation situation is still a very difficult problem in the soft robotic field and no proper methodology has been obtained. The fingertip amplitude of the actuator ranges from −80 mm to 65 mm in the X direction and 0 mm to 110 mm in the Y direction, which has a similar operation space with the human hand[37].

3.2 Gripping objects with different shapes

Fig. 9 shows the pull-off force as a function of various shapes of objects. It is apparent that the shape of the objects has a significant influence on the pull-off force. We divided the shapes of the objects into three groups based on the force values. Group-I (Fig. 9c: the cuboid) generated the minimal pull-off force. Group-II (Figs. 9a and 9b: the sphere and the cylinder) shows the mediate pull-off force. While group-III (Figs. 9d, 9e, and 9f: the cube, the eight-angular prism, and the square

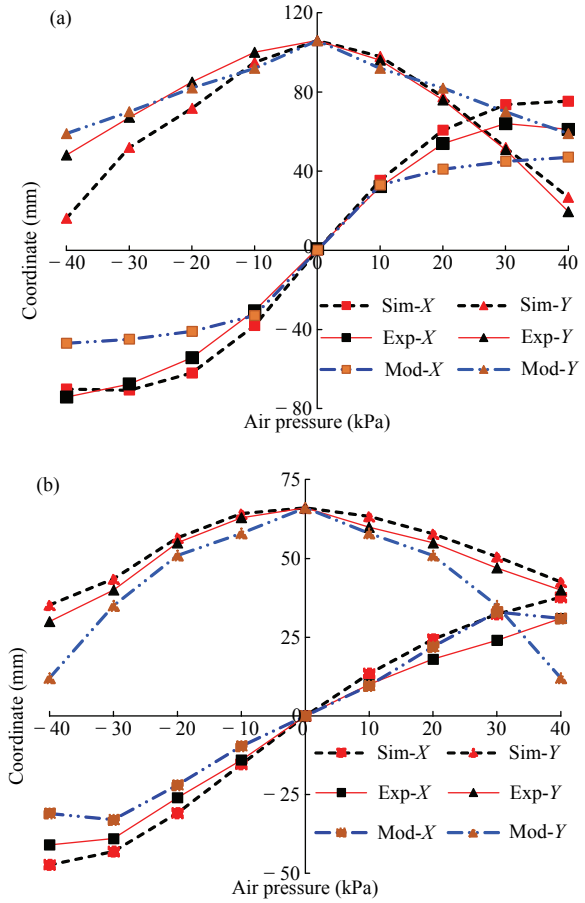

Fig. 8 Tip displacements of the soft actuator vs. air pressure under the FEA simulation, modeling and experiment conditions for (a) the full-length and (b) 50 mm length of the actuator. "Exp-*X*" and "Exp-*Y*" are separately the results of *x* position and *y* position for the experiment. "Sim-*X*" and "Sim-*Y*" are results of FEA simulation. "Mod-*X*" and "Mod-*Y*" are results of the mathematic model.

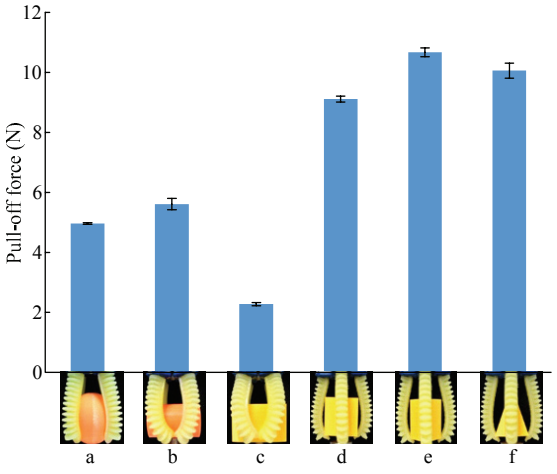

Fig. 9 The pull-off force of the soft gripper as a function of different shapes of objects. a: sphere, b: cylinder, c: cuboid, d: cube, e: eight-angular prism, f: square pyramid.

pyramid) turns out the maximum pull-off force. Concerning the dynamic mechanism of gripping objects, we hypothesize that the gripper achieves its pull-off force through the effects of friction and geometrical interlocking. The experimental data could provide evidence for this hypothesis. In group I (when gripping the cuboid), the gripper deformed and contacted the cuboid on its vertical sides. As the friction force tangential to the surface plays dominated role in the generation of pull-off force, the pull-off force was significantly smaller than those of all the other grasped objects. In contrast, significantly larger pull-off forces were generated in group-III. In this case, the soft gripper deformed and enclosed the objects (see Figs. 9d and 9e) by extending the fingers below the bottom of the objects. A geometrical interlocking effect would take over and dominate the pull-off force, whereas the friction force plays a minor role. As a result, when the robot grips cubic-shaped objects, the maximum pull-off force is around two times larger than that of the sphere-shaped objects. While gripping objects in group II, the soft fingers deformed along the objects' surfaces and generated intermediate pull-off force. However, more scientific analysis of the mechanisms needs to be conducted by combing both theoretical analysis and experiments.

3.3 Speed, error tolerance, and operation precision

Fig. 10 shows the results of actuation speed experiment. From Fig. 10a, it is apparent that the actuation time varies with the shape of the objects, which may be caused by the different gripping strategies for different objects. However, the actuation times for these four objects are approximate, ranging from 0.72 s to 0.92 s. Besides, it can also be seen that the actuation times have little relation to the applied pressures. For all the objects, the gap of the actuation time between the two pressures is 0.04 s. From Fig. 10b, it can be deduced that an object with a bigger size may need more actuation time for the gripper to conform and grip it. The time ranges from 0.56 s (sphere of 40 mm diameter) to 0.92 s (sphere of 60 mm diameter). It could also be concluded from Fig. 10b that the actuation speed should be slower when the soft gripper was operated under the optimal length, for the gripper needs more actuation time to conform the object preferably. However, the time gaps are within

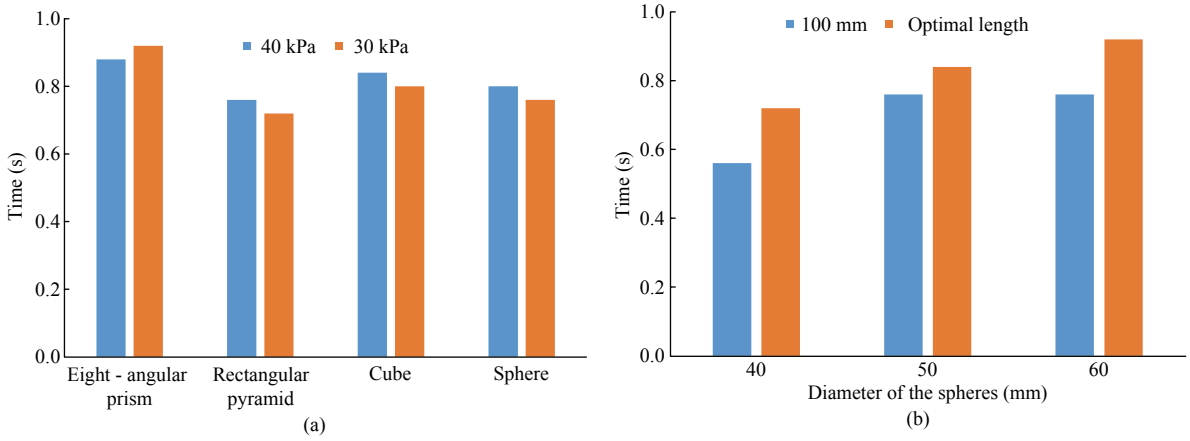

Fig. 10 Test results of actuation times. (a) are the results of actuation time versus the objects' shapes and applied pressures and (b) are results versus the sizes of the objects under different effective actuator lengths.

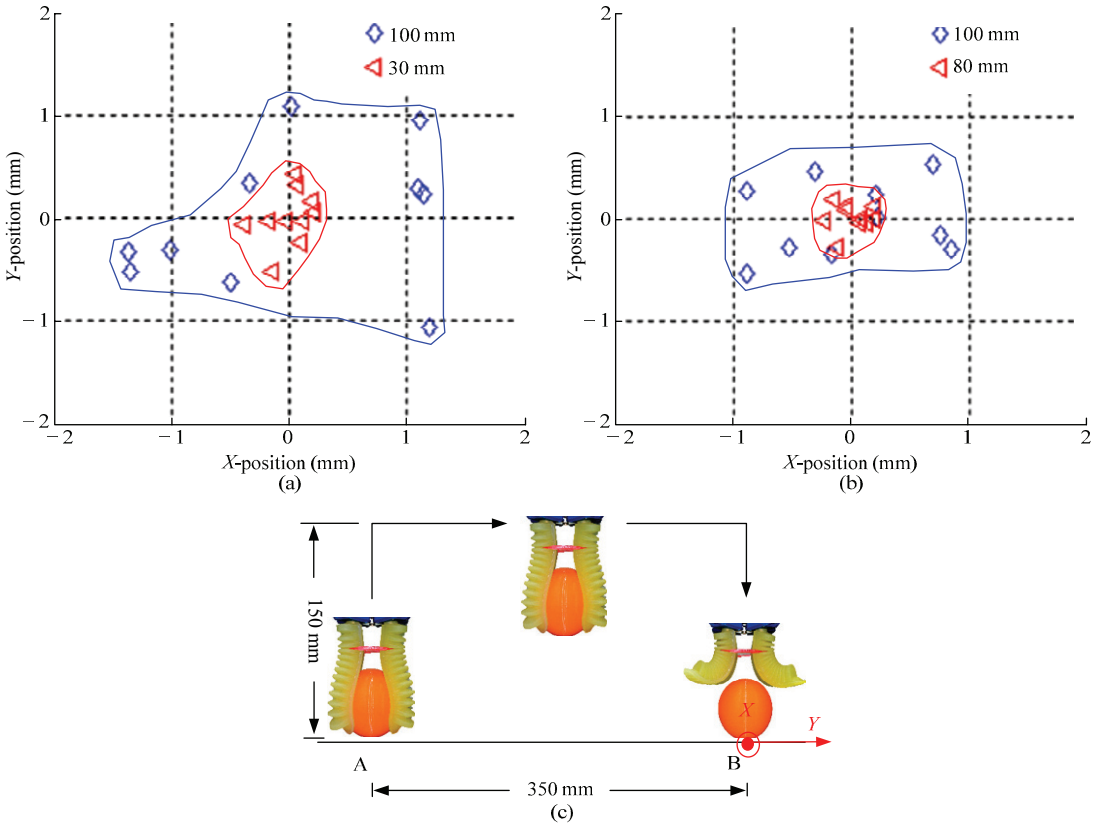

Fig. 11 Pick and placement test results of the soft gripper for different effective actuator lengths. (a) shows the results for the 30 mm diameter sphere and (b) shows the results for the 60 mm diameter sphere. The coordinate system in location B and the moving path are showed in (c).

0.16 s, hardly influencing the efficiency. For all the trials, the actuation times are less than 1 s, which means that the soft gripper has an acceptable actuation speed for the industrial applications.

Fig. 11 shows the precision results of the pick-place experiment. It is evident from both panel a and b that the optimal actuator length can significantly improve the precision for the soft gripper, which is about 2.5 times of that for the full length. For both the two lengths, it can also be found that the precision of placing the 30 mm

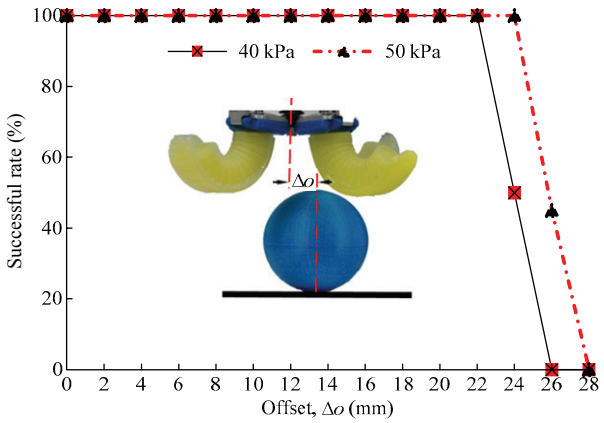

Fig. 12 The successful rate as a function of the offset Δo. "Δo" is the center axis distance between the soft gripper and the sphere.

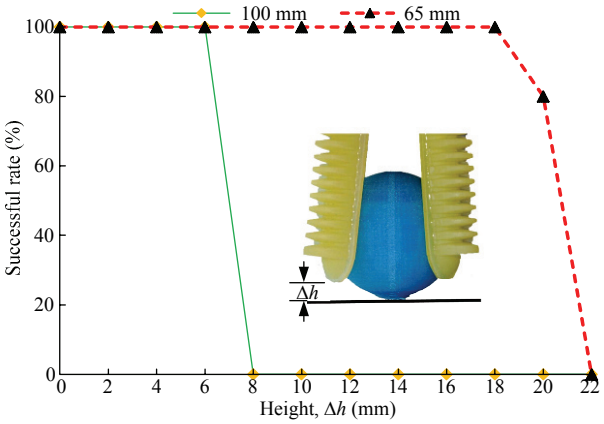

Fig. 13 The successful rate as a function of the distance from fingertips to the ground under different effective lengths. "Δh" is the height from the fingertips to the ground.

diameter sphere is lower than that of placing the 60 mm diameter sphere. However, this difference is not much. Besides, it can be concluded in Fig. 11 that the precision results under the optimal length are within 1.2 mm, which may be a little bigger than the existed rigid industry grippers, but acceptable for the soft gripper properties. The inherent repetitive accuracy of the robot arm is ±0.03 mm, which is tiny for this experiment, so we neglected it. To demonstrate the precision of soft robotic manipulation, in supplementary video S2, we showed that the soft gripper could layer up different objects with holes along a stick, where the diameter of the hole is 6 mm, which is slightly larger than the rod diameter (4 mm)[38].

Fig. 12 and Fig. 13 show the error tolerance of the soft gripper when picking up objects, which present the successful rate vs. the offset and the gripping height respectively. It is apparent from the two curves of Fig. 12 that the successful rate declines drastically when the offset reaches a threshold. For the 40 kPa curve, the threshold is 22 mm. If the pressure increases to 50 kPa, the threshold extends to 24 mm, which means a higher pressure can improve the offset error tolerance. The large error tolerance means that we could depend less on the accuracy demands for the robot arm and control system in real applications. Fig. 13 shows the results of the height error tolerance at two effective actuator lengths of the soft gripper. There also exist thresholds in the two curves. For the 100 mm length curve, the gripper can only pick up the sphere when the height is below 6 mm. However, when the effective actuator length diminishes to 65 mm, the threshold increases to 18 mm, triple that for 100 mm length. The high tolerance for the height may be beneficial in some particular situations, i.e. when the gripper cannot touch the bottom of the object.

The results demonstrated that the precision and error tolerance of the gripper could be significantly improved by using the optimal length of the soft actuator. Under the optimal length, the pick-place precision of the gripper improved by 1.5 times compared to that of the full-length (see Fig. 11 for notation), and the height error tolerance increased by around two times compared to that of the full-length (see Fig. 13 for notation). How can the optimal length improve the gripping performance of the gripper? We speculate that it may be related to two main factors. Firstly, under the optimal length, the gripper can fully conform and contact the surface of the objects, exerting more force on the object. Secondly, the current prototype has vibration during the gripping process. Because the material is soft, the stiffness of the gripper is small. By adding inelastic nylon tendon to the optimal length position of the actuator, the effective length was, in fact, shorter than the full length and the stiffness of the gripper was improved. So the vibration of the gripper during grasping would be significantly reduced.

3.4 Gripping objects with different size and shape

By simply controlling the air pressures and the effective actuator lengths, the soft gripper demonstrates

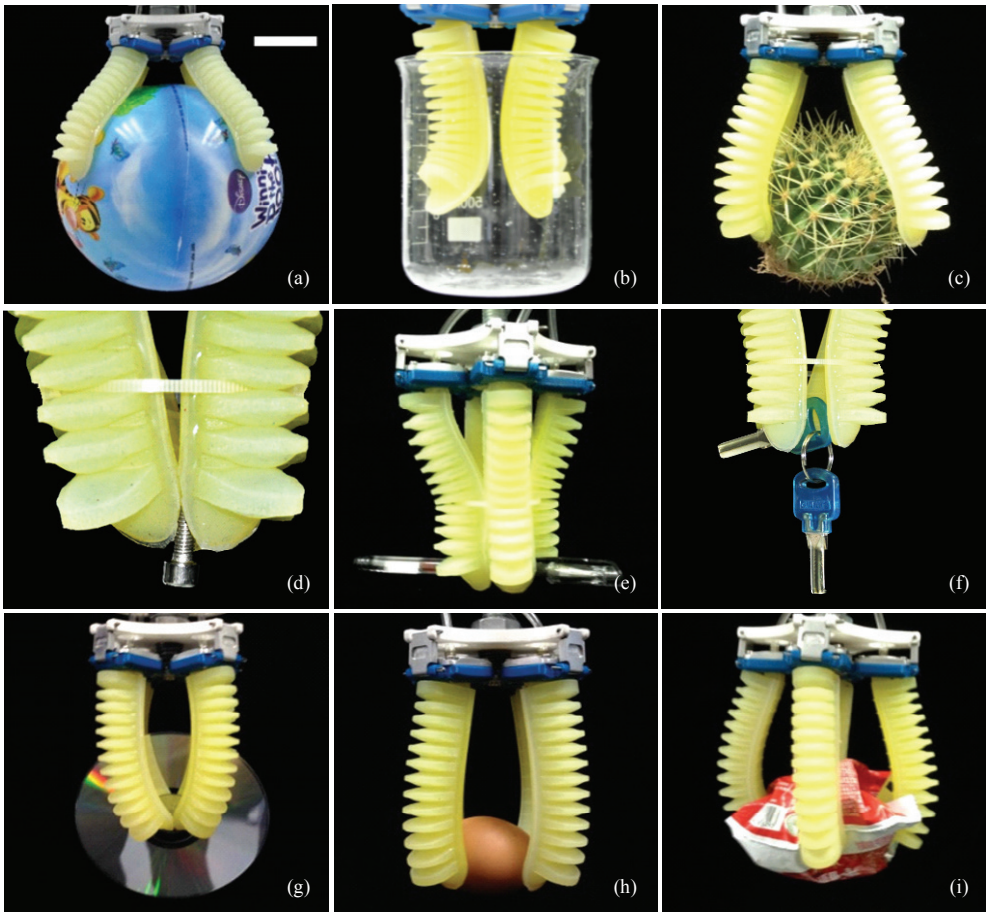

Fig. 14 Results of the universality of the soft gripper. The soft gripper can grasp a sphere with a diameter of 170 mm (a), a beaker (b), a cactus (c), a screw with a diameter of 2 mm (d), a pen (e), a chain of keys (f), a compact disk (g), a raw chicken egg (h), and a bag of milk (i).

the ability to grasp a broad range of objects, including not only those tested objects in Fig. 6 and Fig. 9 but also many other items with different sizes, shapes, and stiffness. For example, the gripper can pick up a sphere with the diameter of 170 mm, over 1.5 times of the length of the single actuator (Fig. 14a). This task is impossible if the gripper cannot bend outwards[27,29]. By operating the gripper under a negative pressure, the gripper can also lift up objects with certain weights by squeezing its inner wall, for example, a beaker with a mass of around 180 g (Fig. 14b). The gripper can also grip a cactus with spines (Fig. 14c), a tiny screw with a diameter of 2 mm (Fig. 14d), a pen (Fig. 14e), or a chain of keys (Fig. 14f). Likewise, it can grip a bag of milk (Fig. 14i), a compact disc (Fig. 14g) and even a raw chicken egg (Fig. 14h). It should be noted that gripping soft, fragile and flatten objects are difficult to achieve by using the traditional robotic grippers and the universal jamming gripper[8,37]. However, it can be achieved by the current soft pneumatic gripper. A video of the prototype gripping multiple objects shown in Fig. 14 is available in the supplementary movie S3. Note that in the video we also showed that the prototype could also grip living organisms, for example, a crab[39].

4 Conclusion

In this article, a pneumatic soft gripper with tunable effective actuator length was presented. By introducing the depressurization mechanism into the soft actuator, the soft gripper can be fully opened, which brings great convenience for grasping large scale objects. Besides, by depressurizing the actuator to a vacuum condition, the time needed to reset the gripper, which took about 0.24 seconds, will be reduced by more than six times com-

pared to the time needed (about 1.5 seconds) by deflating the gripper to the natural state. The design and modeling of the soft actuator were introduced, and effect of the effective actuator length on the gripping performance of the gripper was systematically evaluated by several metrics, i.e., pull-off force, actuation speed, operation precision, and error tolerance. Through the systematic force test, we found that the pull-off force depended on the size of the objects and the effective actuator length. For the object with a particular size, there existed an optimal effective length for the gripper to generate the maximum pull-off force. Apart from the size, the shapes of the objects can also influence the gripping performance. Because the gripper deforms according to the gripped objects, it can achieve the holding force through the effects of both friction and geometrical interlocking. The precision and error tolerance experiments results revealed that the effective actuator length could improve not only the pull-off force but also the precision and error tolerance of the gripper. By setting the effective length to the optimal length, the precision for the pick-place process was improved by 1.5 times and the tolerance for the height error was increased by 2 times, compared to those of the full-length. By tuning the effective actuator length, the gripper can also grasp objects with different sizes, shapes, and stiffness, which was fully demonstrated by the results of the grasping experiment.

For the ongoing work, we are investigating the mechanism to automatically tune the effective lengths to achieve optimal grasping. We are also working on the contact force modeling and force control of the soft robotic gripper, therefore, to extend the capability of the gripper to achieve a more robust and stable working state.

Acknowledgment

This work was supported by the National Science Foundation support projects, China (grant numbers 61633004, 61403012, and 61333016); the Open Research Fund of Key Laboratory Space Utilization, Chinese Academy of Sciences (No.6050000201607004). Many thanks to Ziyu Ren and Hui Wang for their kind help in implementing the experimental apparatus, conducting the force experiments and performing the data analysis. Thanks to Xi Fang for her kind help in revising the paper.

References

[1] Lipson H. Challenges and opportunities for design, simulation, and fabrication of soft robots. *Soft Robotics*, 2014, **1**, 21–27.

[2] Rus D, Tolley M T. Design, fabrication and control of soft robots. *Nature*, 2015, **521**, 467–475.

[3] Kim S, Laschi C, Trimmer B. Soft robotics: A bioinspired evolution in robotics. *Trends in Biotechnology*, 2013, **31**, 23–30.

[4] Ilievski F, Mazzeo A D, Shepherd R F, Chen X, Whitesides G M. Soft robotics for chemists. *Angewandte Chemie*, 2011, **123**, 1930–1935.

[5] Shepherd R F, Stokes A A, Freake J, Barber J, Snyder P W, Mazzeo A D, Cadematiri L, Morin S A, Whitesides G M. Using explosions to power a soft robot. *Angewandte Chemie-International Edition*, 2013, **52**, 2892–2896.

[6] Polygerinos P, Wang Z, Overvelde J T B, Galloway K C, Wood R J, Bertoldi K,Walsh C J. Modeling of soft fiber-reinforced bending actuators. *IEEE Transactions on Robotics*, 2015, **31**, 778–789.

[7] Connolly F, Walsh C J, Bertoldi K. Automatic design of fiber-reinforced soft actuators for trajectory matching. *Proceedings of the National Academy of Sciences of the United States of America*, 2017, **114**, 51.

[8] Brown E, Rodenberg N, Amend J, Mozeika A, Steltz E, Zakin M R, Lipson H, Jaeger H M. Universal robotic gripper based on the jamming of granular material. *Proceedings of the National Academy of Sciences*, 2010, **107**, 18809–18814.

[9] Long J H, Combes S, Nawroth J, Hale M, Lauder G, Swartz S, Quinn R, Chiel H. How does soft robotics drive research in animal locomotion?. *Soft Robotics*, 2014, **1**, 161–168.

[10] Bartlett N W, Tolley M T, Overvelde J T, Weaver J C, Mosadegh B, Bertoldi K Whitesides G M, Wood R J. A 3D-printed, functionally graded soft robot powered by combustion. *Science*, 2015, **349**, 161–165.

[11] Wehner M, Truby R L, Fitzgerald D J, Mosadegh B, Whitesides G M, Lewis J A, Wood R J. An integrated design and fabrication strategy for entirely soft, autonomous robots. *Nature*, 2016, **536**, 451.

[12] Shepherd R F, Ilievski F, Choi W, Morin S A, Stokes A A, Mazzeo A D, Chen X, Wang M, Whitesides G M. Multigait soft robot. *Proceedings of the National Academy of Sciences of the United States of America*, 2011, **108**, 20400–20403.

[13] Morin S A, Shepherd R F, Kwok S W, Stokes A A, Nemiroski A, Whitesides G M. Camouflage and display for soft

machines. *Science*, 2012, **337**, 828–832.

[14] Shepherd R F, Stokes A A, Nunes R M, Whitesides G M. Soft machines that are resistant to puncture and that self seal. *Advanced Materials*, 2013, **25**, 6709–6713.

[15] Cho K J, Koh J S, Kim S, Chu W S, Hong Y, Ahn S H. Review of manufacturing processes for soft biomimetic robots. *International Journal of Precision Engineering and Manufacturing*, 2009, **10**, 171–181.

[16] Stokes A A, Shepherd R F, Morin S A, Ilievski F, Whitesides G M. A hybrid combining hard and soft robots. *Soft Robotics*, 2014, **1**, 70–74.

[17] Connolly F, Polygerinos P, Walsh C J, Bertoldi K. Mechanical programming of soft actuators by varying fiber angle. *Soft Robotics*, 2015, **2**, 26–32.

[18] Odhner L U, Jentoft L P, Claffee M R, Corson N, Tenzer Y, Ma R R, Buehler M, Kohout R, Howe R D, Dollar A M. A compliant, underactuated hand for robust manipulation. *International Journal of Robotics Research*, 2014, **33**, 736–752.

[19] Stuart H S, Wang S, Gardineer B, Christensen D L, Aukes D M, Cutkosky M. A compliant underactuated hand with the suction flow for underwater mobile manipulation. *Robotics and Automation* (*ICRA*), 2014 *IEEE International Conference on*, Hong Kong, China, 2014, 6691–6697.

[20] Mosadegh B, Polygerinos P, Keplinger C, Wennstedt S, Shepherd R F, Gupta U, Shim J, Bertoldi K, Walsh C J, Whitesides G M. Soft robotics: Pneumatic networks for soft robotics that actuate rapidly. *Advanced Functional Materials*, 2014, **24**, 2163–2170.

[21] Girard A, Bigué J P L, O'Brien B M, Gisby T A, Anderson I A, Plante J. Soft two-degree-of-freedom dielectric elastomer position sensor exhibiting linear behavior. *IEEE/ASME Transactions on Mechatronics*, 2015, **20**, 105–114.

[22] Shen Q, Wang T, Liang J, Wen L. Hydrodynamic performance of a biomimetic robotic swimmer actuated by 02ionic polymer–metal composite. *Smart Materials & Structures*, 2013, **22**, 075035.

[23] Park Y L, Chen B R, Pérezarancibia N O, Young D, Stirling L, Wood R J, Goldfield E C, Nagpal R. Design and control of a bio-inspired soft wearable robotic device for ankle-foot rehabilitation. *Bioinspiration & Biomimetics*, 2014, **9**, 16007–16023.

[24] Ding Y, Galiana I, Asbeck A, Quinlivan B, Rossi S M M D, Walsh C. Multi-joint actuation platform for lower extremity soft exosuits. 2014 *IEEE International Conference on Robotics and Automation* (*ICRA*), Hong Kong, China, 2014, 1327–1334.

[25] Calisti M, Giorelli M, Levy G, Mazzolai B, Hochner B, Laschi C, Dario P. An octopus-bioinspired solution to movement and manipulation for soft robots. *Bioinspiration & Biomimetics*, 2011, **6**, 525–531.

[26] Onal C D, Rus D. Autonomous undulatory serpentine locomotion utilizing body dynamics of a fluidic soft robot. *Bioinspiration & Biomimetics*, 2013, **8**, 653–668.

[27] Homberg B S, Katzschmann R K, Dogar M R, Rus D. Haptic identification of objects using a modular soft robotic gripper. 2015 *IEEE/RSJ International Conference on Intelligent Robots and Systems* (*IROS*), Hamburg, Germany, 2015, 1698–1705.

[28] Deimel R, Brock O. A novel type of complaint, underactuated robotic hand for dexterous grasping. *International Journal of Robotics Research*, 2015, **35**, 161–185.

[29] Wang B, McDaid A, Giffney T, Biglariabhari M, Aw K C. Design, modeling and simulation of soft grippers using new bimorph pneumatic bending actuators. *Cogent Engineering*, 2017, **4**, 1285482.

[30] Hao Y, Wang T, Ren Z, Gong Z, Wang H, Yang X, Guan S, Wen L. Modeling and experiments of a soft robotic gripper in amphibious environments. *International Journal of Advanced Robotic Systems*, 2017, **14**, 1729881417707148.

[31] Shuichi W, Koichi S, Keiko O. Miniature pneumatic curling rubber actuator generating bidirectional motion with one air-supply tube. *Advanced Robotics*, 2011, **25**, 1311–1330.

[32] Lessing J A, Knopf R R, Mclellan N. *Soft Robotic Actuators Utilizing Asymmetric Surfaces*, U S Patent, No. US20160114482 A1, 28 Apr. 2016.

[33] Hong K Y, Hui Y N, Yeow C H. High-force soft printable pneumatics for soft robotic applications. *Soft Robotics*, 2016, **3**, 144–158.

[34] https://v.qq.com/x/page/h0394k0nk37.html, [2017-04-19].

[35] Manti M, Hassan T, Passetti G, NicolòD'Elia, Laschi C, Cianchetti M. A Bioinspired soft robotic gripper for adaptable and effective grasping. *Soft Robotics*, 2015, **2**, 107–116.

[36] Timoshenko S P, Woinowsky-Krieger S. *Theory of Plates and Shells*, McGraw-hill, New York, USA, 1959.

[37] Amend J R, Brown E, Rodenberg N, Jaeger H M, Lipson H. A positive pressure universal gripper based on the jamming of granular material. *IEEE Transactions on Robotics*, 2012, **28**, 341–350.

[38] https://v.qq.com/x/page/g0394x42ko9.html, [2017-04-19].

[39] https://v.qq.com/x/page/n03942sh079.html, [2017-04-19].